Phase diagram and optimal switching induced by spin Hall effect in a perpendicular magnetic layer

Shu Yan and Ya. B. Bazaliy

Phys. Rev. B **91**, 214424 — Published 17 June 2015

DOI: 10.1103/PhysRevB.91.214424

Phase diagram and optimal switching induced by spin Hall effect in a perpendicular magnetic layer

Shu Yan[1,*] and Ya. B. Bazaliy[1,†]

[1] *Department of Physics and Astronomy, University of South Carolina, Columbia, South Carolina 29208*

(Dated: June 1, 2015)

In a ferromagnet/heavy-metal bilayer device with strong spin Hall effect an in-plane current excites magnetic dynamics through spin torque. We analyze bilayers with perpendicular magnetization and calculate three-dimensional phase diagrams describing switching by external magnetic field at a fixed current. We then concentrate on the case of a field applied in the plane formed by the film normal and the current direction. Here we analytically study the evolution of both the conventional "up"/"down" magnetic equilibria and the additional equilibria created by the spin torque. Expressions for the stability regions of all equilibria are derived, and the nature of switching at each critical boundary is discussed. The qualitative picture obtained this way predicts complex hysteresis patterns that should occur in bilayers. Analyzing the phase portraits of the system we find regimes where switching between the "up" and "down" states proceeds through the current-induced state as an intermediate. The first step of such two-step process is fast and resembles ballistic switching for the reasons discussed in the paper. Using numeric simulations we analyze the switching time and compare it to that of a conventional spin torque device with collinear magnetizations of the polarizer and the free layer.

I. INTRODUCTION

Recently a number of investigations focused on bilayer structures consisting of a ferromagnetic (F) layer and a nonmagnetic (N) layer with strong spin-orbit (SO) interaction made of heavy-metals such as Pt, Ta or W.[1–10] It was theoretically predicted and experimentally observed that when an in-plane electric current is being applied, the itinerant electrons inside the nonmagnetic layers become spin polarized due to the strong spin-orbit coupling and exert a spin torque on the ferromagnetic layers. This additional torque contributes to the magnetization dynamics described by the Landau-Lifshitz-Gilbert (LLG) equation. Up to now two models have been proposed to account for the effects. One of them[2,5] treats the bilayer structure as a two-dimensional system with strong interfacial Rashba spin-orbital coupling due to the structural inversion symmetry breaking in the direction normal to the interface.[11] This model leads to a field-like torque directed along $\hat{\mathbf{m}} \times (\mathbf{j}_e \times \hat{\mathbf{z}})$,[12–16] where $\hat{\mathbf{m}} = \mathbf{M}/M_s$ is the magnetization unit vector (M_s represents the constant absolute value of the magnetization $\mathbf{M}$), $\mathbf{j}_e$ is the in-plane electric current density, and $\hat{\mathbf{z}}$ is a unit vector perpendicular to the plane of the layers. The other model[1,4,6–9] is based on the interfacial diffusion of the pure spin current that originates in the heavy-metal layers due to the bulk spin Hall effect (SHE)[17–20] and leads to spin transfer torque (STT) dynamics[21,22] in the magnetic layers. In the SHE model the torque is directed along $\hat{\mathbf{m}} \times [\hat{\mathbf{m}} \times (\mathbf{j}_e \times \hat{\mathbf{z}})]$.[23] This type of torque is called a Slonczewski, or damping-like, or adiabatic torque in the literature.

Several experiments showed that an in-plane electric current flowing through the structure is able to switch the magnetization of the ferromagnetic layer.[5,7–9] In those experiments the F layers were magnetized perpendicular to the film plane. It is believed that the observed magnetic reversal can only be induced by the damping-like torque. The reasons for this are (a) experimentally measured switching phase diagrams are in accord with the macrospin model calculations[7,24], and (b) due to its symmetry, a field-like torque, if there is any, does not favor either "up" or "down" state of the perpendicular magnetization, and therefore should not contribute to switching. These arguments seem to favor the SHE-based model, however, subsequent calculations[25–27] suggested that the model based on Rashba coupling generates both field-like and damping-like torques, and thus is also capable of describing the switching.

Despite the fact that the underlying torque mechanism is still not fully understood, a thorough study of the switching behavior is of importance for analysis and prediction. In this paper we perform such a study describing the magnetic layer within the framework of a macrospin model. This is a reasonably good approximation when the sample size is small enough for the magnetization to be close to uniform. In larger samples the situation may be different and recent experiments have shown that domain nucleation[28] and propagation[24,29,30] need to be

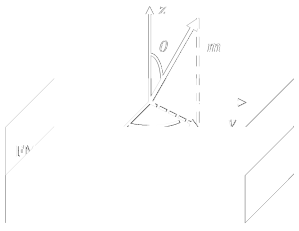

FIG. 1. Schematic diagram of the bilayer spin Hall effect device. Electric current j flows along the y axis.

taken into account in those cases. With macrospin approximation in place, our goal will be to describe magnetic switching induced by an externally applied field $\mathbf{H}$ at a fixed in-plane electric current. It will be further assumed that the magnetic anisotropy energy of the F layer corresponds to an easy axis directed normal to the layers (perpendicular anisotropy)

$$E(\mathbf{m}) = -K(\hat{\mathbf{m}} \cdot \hat{\mathbf{z}})^2. \quad (1)$$

Magnetization is switched between the "up" and "down" states at critical fields $\mathbf{H}_c$ that form a surface in three-dimensional H-space. Without electric current and for the magnetic anisotropy given by (1) this surface is an axially symmetric figure of revolution with a cross-section given by the astroid curve.[31] The presence of the in-plane current $\mathbf{j}_e$ breaks the axial symmetry through the damping and the field-like spin torques. However, the field-like torque can be compensated by an external field in $\mathbf{j}_e \times \hat{\mathbf{z}}$ direction, thus, its presence simply shifts the entire critical surface without changing its shape. For the purpose of finding the shape of the current-modified astroid we may consider the damping torque alone.

In this paper we calculate the 3D critical surface in H-space using the method of Refs. 32 and 33. Astroid modification in the same setting was previously studied in Refs.7, 34–36 Earlier analytic studies dealt with the properties of equilibria that exist at zero current and are modified when the spin torque is turned on. This paper provides results on the novel equilibria that are produced by the current. The evidence for their existence was previously obtained numerically[37] but an in-depth study of their properties, including their role in magnetic switching, was lacking.

The outline of the paper is as follows. In Sec. II we review the theoretical approach of Refs. 32 and 33. In Sec. III we find the three-dimensional $\mathbf{H}_c$ at a given current magnitude and give analytic formulas for this multi-sheet surface. However, the surface itself does not provide all the details of switching. To understand them one has to determine which equilibria are destabilized on each of its sheets. In Sec. IV, we perform such an analysis for a particular cross-section of the critical surface, the one with $\mathbf{H}$ confined to the plane formed by the electric current $\mathbf{j}_e$ and the film normal $\hat{\mathbf{z}}$. After resolving the implicit 3D analytic expressions, we find the corresponding 2D cross-section of $\mathbf{H}_c$. We further observe, in accord with the previous numeric investigations,[37] that sufficiently large currents produce an extra equilibrium in addition to the existing "up" and "down" ones. Analytical expressions are derived for the position and stability region of this equilibrium. Knowing the equilibrium states of the system, we provide the description of all possible switching events and discuss the usage of the modified astroid in various experimental situations. In Sec. V, we analyze the phase portraits of the system and study its evolution after the destabilization of a given equilibrium. Here we show that the extra equilibrium plays an important role in the switching process, influencing its speed and fashion.

II. GENERAL DESCRIPTION OF THE THEORETICAL APPROACH

Magnetization dynamics of the ferromagnetic layer in the macrospin approximation is governed by the LLG equation:

$$\frac{d\mathbf{M}}{dt} = -\gamma\mu_0(\mathbf{M} \times \mathbf{H}_{\text{eff}}) + \frac{\alpha}{M_s}\left(\mathbf{M} \times \frac{d\mathbf{M}}{dt}\right), \quad (2)$$

where α is the Gilbert damping factor, γ is the gyromagnetic ratio, and $\mathbf{H}_{\text{eff}}$ is the total effective field. The standard LLG equation can be transformed into

$$\frac{d\hat{\mathbf{m}}}{dt} = -\hat{\mathbf{m}} \times \mathbf{h}_{\text{eff}} - \alpha\hat{\mathbf{m}} \times \hat{\mathbf{m}} \times \mathbf{h}_{\text{eff}}, \quad (3)$$

where the field is rescaled as $\mathbf{h}_{\text{eff}} = \mathbf{H}_{\text{eff}}/H_k$ using the characteristic anisotropy field $H_k = 2K/\mu_0 M_s$, and the time is rescaled as $t \to t' = \gamma\mu_0 H_k t/(1+\alpha^2)$. Hereafter, all the field-related terms that are written in lowercase letters are dimensionless (normalized by H_k).

The method used to find the critical surfaces[32,33] can be summarized as follows. A stationary solution $\hat{\mathbf{m}}_0$ of Eq. (3) satisfies the equilibrium condition $\hat{\mathbf{m}} \times \mathbf{h}_{\text{eff}} = 0$, which indicates that the magnetization at equilibrium should be parallel to the total effective field, i.e., $\mathbf{h}_{\text{eff}} = \lambda\hat{\mathbf{m}}_0$ with arbitrary λ. Total effective field is given by $\mathbf{h}_{\text{eff}} = \mathbf{h} - \nabla\varepsilon + \mathbf{h}_{\text{sp}}$, where $\mathbf{h}$ is the external field, $\varepsilon = E/(\mu_0 H_k M_s)$ is the rescaled anisotropy energy, and $\mathbf{h}_{\text{sp}}$ is the spin torque effective field

$$\mathbf{h}_{\text{sp}} = \alpha_j[\mathbf{m} \times (\mathbf{e}_j \times \hat{z})], \quad (4)$$

where $\mathbf{e}_j$ is a unit vector in the electric current direction and α_j is a spin torque strength parameter, proportional to the electric current density. Equation $\mathbf{h}_{\text{eff}} = \lambda\hat{\mathbf{m}}_0$ can be solved for the external field as $\mathbf{h} = \lambda\mathbf{m}_0 + \nabla\varepsilon(\mathbf{m}_0) - \mathbf{h}_{sp}(\mathbf{m}_0)$. The meaning of this formula is that for any given magnetization direction there is a whole line of external fields, parameterized by λ, which make it an equilibrium — stable or unstable. In spherical coordinates with three orthogonal unit vectors defined as $\hat{\mathbf{m}} = \sin\theta\cos\phi\hat{\mathbf{x}} + \sin\theta\sin\phi\hat{\mathbf{y}} + \cos\theta\hat{\mathbf{z}}$, $\hat{\theta} = \partial\hat{\mathbf{m}}/\partial\theta$, and $\hat{\phi} = (1/\sin\theta)\partial\hat{\mathbf{m}}/\partial\phi$, we get

$$\mathbf{h} = \lambda\hat{\mathbf{m}}_0 + \left(\partial_\theta\varepsilon - h^\theta_{\text{sp}}\right)_0\hat{\theta}_0 + \left(\frac{1}{\sin\theta}\partial_\phi\varepsilon - h^\phi_{\text{sp}}\right)_0\hat{\phi}_0\ , \quad (5)$$

where ∂_θ stands for $\partial/\partial\theta$ and the superscript θ indicates the $\hat{\theta}$ component of a vector field (e.g., $h^\theta_{\text{eff}} = \mathbf{h}_{\text{eff}} \cdot \hat{\theta}$), etc. Equation (5) maps the 3D space $\{\lambda, \theta_0, \phi_0\}$ to the 3D field space $\{h_x, h_y, h_z\}$.

Next, stability of equilibrium states is analyzed. This is done by expanding Eq. (3) in small deviations $\hat{\mathbf{m}} =$

$\hat{\mathbf{m}}_0 + \delta\hat{\mathbf{m}}$ up to the linear terms. Such an expansion produces two coupled linear differential equations

$$\begin{pmatrix} \dot{\delta\theta} \\ \sin\theta_0 \dot{\delta\phi} \end{pmatrix} = A\left(\theta_0, \phi_0\right) \begin{pmatrix} \delta\theta \\ \sin\theta_0 \delta\phi \end{pmatrix}, \tag{6}$$

with matrix $A(\theta_0, \phi_0)$ given by

$$A = \begin{bmatrix} \partial_\theta(\alpha h^\theta_{\rm eff} + h^\phi_{\rm eff}) & \frac{1}{\sin\theta}\partial_\phi(\alpha h^\theta_{\rm eff} + h^\phi_{\rm eff}) \\ \partial_\theta(\alpha h^\phi_{\rm eff} - h^\theta_{\rm eff}) & \frac{1}{\sin\theta}\partial_\phi(\alpha h^\phi_{\rm eff} - h^\theta_{\rm eff}) \end{bmatrix} \tag{7}$$

Stationary solutions can be classified as stable or unstable using the eigenvalues of A. For a 2×2 matrix the two eigenvalues $\mu_\pm$ are uniquely determined by its determinant, $\det A$, and trace, $\mathrm{tr}A$.[38] An equilibrium is stable when both eigenvalues $\mu_\pm$ are either complex numbers with negative real parts, or negative real numbers, which leads to the stability criterion

$$\det A > 0 \text{ and } \mathrm{tr}A < 0\ . \tag{8}$$

For a given direction (θ_0, ϕ_0) this criterion selects the parts of the field line $\mathbf{h}(\lambda, \theta_0, \phi_0)$ (5) for which (θ_0, ϕ_0) is not just an equilibrium but specifically a stable equilibrium. Those stable parts are specified by the intervals of λ where conditions (8) are satisfied. By evaluating expression (7) at external field specified by Eq. (5) one obtains $A(\lambda)$. We find that for the arbitrary form of spin torque and arbitrary anisotropy energy, $\mathrm{tr}A(\lambda)$ is a linear function λ with a negative linear coefficient, and $\det A(\lambda)$ is a quadratic function of λ with a positive quadratic coefficient. To simplify the expressions, we introduce a vector field $\mathbf{f} = -\nabla\varepsilon + \mathbf{h}_{\rm sp}$ and its matrix gradient

$$\nabla\mathbf{f} \equiv \begin{bmatrix} \partial_\theta f^\theta & \partial_\theta f^\phi \\ \partial_\phi f^\theta & \partial_\phi f^\phi \end{bmatrix} \tag{9}$$

(see Appendix A for the explicit expressions). The roots of equations $\mathrm{tr}A(\lambda) = 0$ and $\det A(\lambda) = 0$ can be respectively calculated as

$$\lambda_{\rm T}(\theta_0, \phi_0) = \frac{1}{2}\left[\partial_\theta f^\theta + \partial_\phi f^\phi + \frac{1}{\alpha}\left(\partial_\theta f^\phi - \partial_\phi f^\theta\right)\right], \tag{10}$$

$$\lambda_\pm(\theta_0, \phi_0) = \frac{\partial_\theta f^\theta + \partial_\phi f^\phi}{2} \pm\sqrt{\left(\frac{\partial_\theta f^\theta - \partial_\phi f^\phi}{2}\right)^2 + \partial_\theta f^\phi \partial_\phi f^\theta}. \tag{11}$$

In terms of the critical values $\lambda_{\rm T}$ and $\lambda_\pm$, the stability criteria become

$$\begin{cases} \lambda > \mathrm{Max}(\lambda_{\rm T}, \lambda_+) & \text{if } \lambda_{\rm T} \geqslant \lambda_-, \\ \lambda_{\rm T} < \lambda < \lambda_- \text{ or } \lambda > \lambda_+ & \text{if } \lambda_{\rm T} < \lambda_-. \end{cases} \tag{12}$$

When $\lambda_\pm$ are complex, $\det A$ is always positive and criteria (12) can be further simplified as $\lambda > \lambda_{\rm T}$. The full classification is given in Appendix B.

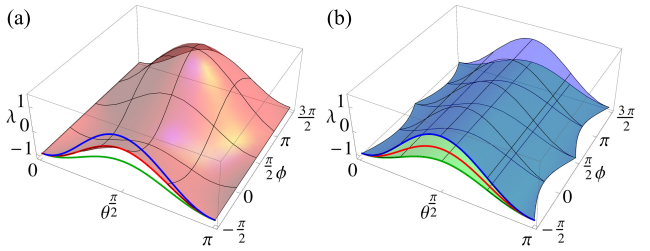

FIG. 2. (color online) Illustrative example of critical values (a) $\lambda_{\rm T}$(red) and (b) $\lambda_{+/-}$(blue/green) as functions of (θ, ϕ) for $\alpha = 0.1$ and $\alpha_{\rm j} = 0.1$. Zero current critical values (independent of ϕ) are plotted for reference as additional lines at $\phi = -\pi/2$ using the same color convention. For consistency, same parameters and color convention are used in the remaining figures in this section.

Substituting functions λ_+, λ_- or $\lambda_{\rm T}$ for λ in Eq. (5) one generates three surfaces in the field space, which are denoted S_+, S_- and $S_{\rm T}$ respectively. Their physical meaning is that at least one equilibrium changes its stability when external field crosses such a surface. It is either locally destabilized when the $S_{\rm T}$ surface is crossed, or merges with a saddle point when the $S_\pm$ surfaces are crossed.[39] The entire critical surface S is constructed from the parts of S_+, S_- and $S_{\rm T}$ as explained in Ref. 33.

III. 3D PHASE DIAGRAM

In this section we construct the three-dimensional critical surface using the method of Sec. II. The dimensionless perpendicular anisotropy energy has the form $\varepsilon = -\cos^2\theta/2$. We set the in-plane current to be along the $+\hat{\mathbf{y}}$ direction, and the current induced field is then $\mathbf{h}_{\rm sp} = \alpha_j \hat{\mathbf{m}} \times \hat{\mathbf{x}}$ with α_j given by $\alpha_j = \theta_{\rm SH} j_{\rm e}/j_0$, where $\theta_{\rm SH}$ is the spin Hall angle, $j_0 = 2eM_{\rm s}d_{\rm F}H_k/\hbar$ is the characteristic current density, and $d_{\rm F}$ is the thickness of the F layer. For brevity, we drop index "0" for the equilibrium direction. The critical values of λ calculated according to (10) and (11) specialize to

$$\lambda_{\rm T}(\theta, \phi) = \frac{\sin^2\theta}{2} - \cos^2\theta - \frac{\alpha_{\rm j}}{\alpha}\sin\theta\cos\phi, \tag{13}$$

$$\lambda_\pm(\theta, \phi) = \frac{\sin^2\theta}{2} - \cos^2\theta \pm \sin\theta\sqrt{\frac{\sin^2\theta}{4} - \alpha_j^2\cos^2\phi}. \tag{14}$$

Fig. 2 shows three critical values as functions of equilibrium angles at nonzero current with $\alpha_j = 0.1$ and $\alpha = 0.1$.

For practical calculations we decompose Eq. (5) into Cartesian coordinates

$$h_x = (\lambda + \cos^2\theta)\sin\theta\cos\phi, \tag{15a}$$

$$h_y = (\lambda + \cos^2\theta)\sin\theta\sin\phi - \alpha_j\cos\theta, \tag{15b}$$

$$h_z = (\lambda - \sin^2\theta)\cos\theta + \alpha_j\sin\theta\sin\phi. \tag{15c}$$

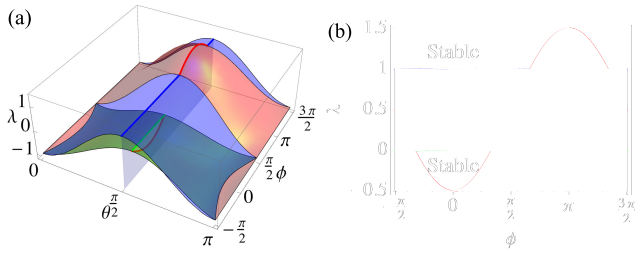

FIG. 3. (color online) Selection of relevant λ surfaces: (a) 3D view of the λ_T and $\lambda_\pm$ surfaces and (b) the cross-section at $\theta = \pi/2$. The relevant surfaces separate stable and unstable values of λ, as illustrated by solid lines in (b).

For an arbitrary λ these equations represent the mapping of the (λ, θ, ϕ) space to the (h_x, h_y, h_z) space for the case of uniaxial anisotropy and chosen electric current direction. When functions $\lambda_{\rm T}(\theta, \phi)$ (13) or $\lambda_\pm(\theta, \phi)$ (14) are substituted for λ, one obtains parametric expressions for the critical surfaces $S_{\rm T}$ and $S_\pm$ with parameters (θ, ϕ) running through all possible values, $0 \leqslant \theta \leqslant \pi$ and $0 \leqslant \phi \leqslant 2\pi$.

For each (θ, ϕ) one has to choose the relevant S surfaces[33] that correspond to critical λ's bracketing the stability intervals (12). For example, for $\alpha_j = 0$ one finds $\lambda_{\rm T}$ to be in the midpoint of the interval (λ_-, λ_+) for any direction (θ, ϕ), and therefore only S_+ is relevant and constitutes the entire critical surface. For non-zero current $\lambda_{\rm T}$ may leave the interval (λ_-, λ_+) for some values of (θ, ϕ). In those cases destabilization boundaries should be selected for every direction individually. The selection of relevant critical λ surfaces is illustrated in Fig. 3.

By substituting the relevant critical λ values into equations (15), we plot the critical surface S as shown in Fig. 4. Three types of modifications due to spin torque can be observed. First, the original astroid is distorted forming the blue region bounded by the S_+ surface. Second, part of the S_+ surface, where $\lambda_{\rm T} > \lambda_+$ is satisfied, becomes irrelevant. A red region in the figure is formed this way. Third, extra equilibrium points appear in the field space where $\lambda_{\rm T} < \lambda_-$ is satisfied, forming the green region. While the task of constructing S is achieved, its interpretation requires more work. Critical surface can be a complicated self-crossing manifold.[33] To understand it one has to specify which equilibrium is destabilized at each surface, and on which side of the surface is this equilibrium stable. A corresponding study for one cross-section of S is given in the next section.

IV. PHASE DIAGRAM IN THE Y-Z PLANE

The 3D phase diagram is quite difficult to use due to the complicated shape of the critical surface S. Moreover, experiments are often performed with the field being confined within the $y - z$ plane.[7,24] Here we study in detail a section of S corresponding to the external field

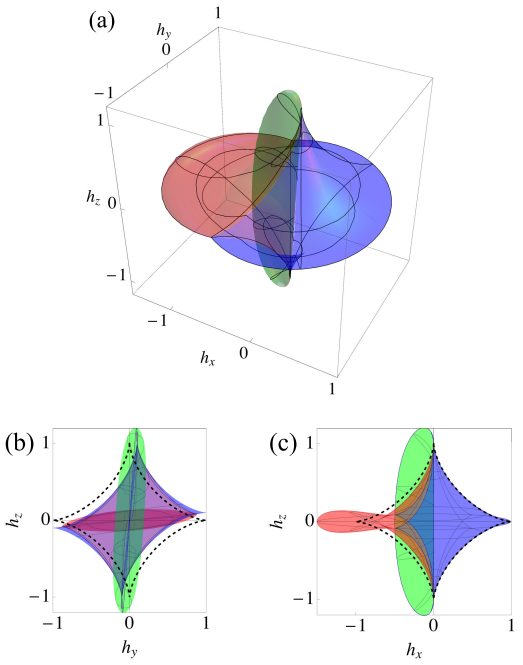

FIG. 4. (color online) Critical surface S: (a) 3D view; (b) side view along x axis; (c) side view along y axis. For reference purposes the conventional Stoner-Wohlfarth (SW) astroid is plotted in (b) and (c) using a dashed black line. The same color convention and parameters as in Fig. 2 are adopted.

h confined to such a plane. This section is a line $\bar{S}$ in the 2D space (h_y, h_z). Note that if a field-like component spin torque is present in the system, it has to be compensated by an appropriate constant h_x component of external field in order for our results to be applicable.

A field in the $y - z$ plane satisfies a constraint $h_x = 0$. According to Eq. (15a) this implies a relationship between θ, ϕ, and λ. On the one hand, this relationship allows one to express the equilibrium angles (θ, ϕ) as functions of (h_y, h_z) and study how the equilibria evolve as a function of applied field. On the other hand, Eq. (15a) can be used to find the section $\bar{S}$. While the surface S is given by a parametric formula with independently varying θ and ϕ as explained in Sec. III, the line $\bar{S}$ is found from the same formula with θ and ϕ being related to each other by a requirement that Eq. (15a) holds with $\lambda = \lambda_{T,+,-}(\theta, \phi)$.

A. Evolution of equilibrium states

Equation (15a) has three types of solutions: (I) $\phi = \pm\pi/2$, (II) $\lambda = -\cos^2\theta$, and (III) $\theta = 0, \pi$. Since the value of ϕ at $\theta = 0, \pi$ is immaterial, type III can be considered as a special case of type I. Thus we focus on the first two cases. For definiteness, assume $\alpha_j > 0$.

Solutions of type I have $\sin\phi = \pm 1$. They are located on the meridian of the unit sphere lying in the $y-z$ plane. We will call them on-meridian states. Eliminating λ from

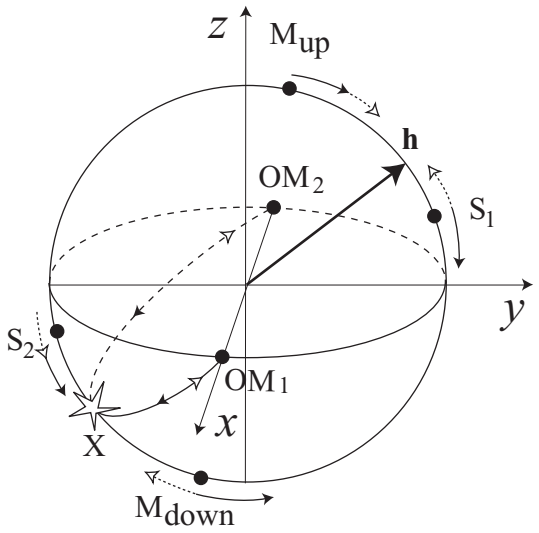

FIG. 5. Equilibrium states shown as points on the unit sphere for small current $\alpha_j > 0$ and field $\mathbf{h}$. Solid arrows show equilibria displacements as h is increased at fixed α_j. Dashed empty arrows show equilibria displacements as α_j is increased at fixed h. For example, increasing field at fixed current causes an eventual merging of points OM_1, OM_2, and S_2 that produces point X.

Eqs. (15b) and (15c) one finds a system of equations for their polar angles

$$\phi = \pm\pi/2 \ ,$$
$$h_y \cos\theta \mp h_z \sin\theta = \pm \sin\theta\cos\theta - \alpha_j. \qquad (16)$$

Depending on h_y, h_z and α_j there can be four, two or zero equilibrium states of type I.

Solutions of type II have $\lambda = -\cos^2\theta$. Equations (15b) and (15c) read

$$h_y = -\alpha_j \cos\theta,$$
$$h_x = -\cos\theta + \alpha_j \sin\theta \sin\phi.$$

Solving them one finds

$$\cos\theta = -\frac{h_y}{\alpha_j}, \qquad (17)$$
$$\sin\phi = \frac{h_z - h_y/\alpha_j}{\sqrt{\alpha_j^2 - h_y^2}}$$

with associated requirements $|h_y| \le \alpha_j$ and $|(h_z - h_y/\alpha_j)/\sqrt{\alpha_j^2 - h_y^2}| \le 1$ that define their domain of existence. Having $\phi \neq \pm\pi/2$, type II solutions are away from the $y-z$ plane and will be called off-meridian states. They exist as a pair with the same polar angle θ and azimuthal angles ϕ and $\pi - \phi$.

Equilibrium states can be visualized as points on the unit sphere that change their positions when the experimental parameters $\mathbf{h}$ and α_j are varied (Fig. 5). In the absence of current and external field the uniaxial magnet exhibits two stable equilibria $\theta = 0, \pi$: the "up" and "down" states. Due to the axial symmetry of the system the entire equator of the unit sphere forms a circle of unstable equilibrium states.

At non-zero current spin torque breaks the axial symmetry of the problem even in the absence of magnetic field. For $\alpha_j \neq 0$, $\mathbf{h} = 0$ the continuous set of unstable equilibria along the sphere's equator is reduced to four isolated equilibrium points. Two of them are off-meridian states ($OM_{1,2}$ in Fig. 5) for which Eq. (17) gives $\theta = \pi/2$ and $\phi = 0, \pi$, i.e., the $\pm\hat{x}$ directions. The other two are on-meridian states $S_{1,2}$ given by Eq. (16). It will be shown below that they are saddle points. For small α_j the system has six equilibria: slightly displaced "up" (M_{up}) and "down" (M_{down}) on-meridian states, on-meridian states $S_{1,2}$ that are slightly displaced from the equator of the sphere, and the $\pm\hat{x}$ states $OM_{1,2}$ (Fig. 5).

The following useful rules apply to the on-meridian equilibria described by Eq. (16): (1) Increasing current shifts points $M_{up/down}$ clockwise and points $S_{1,2}$ counterclockwise along the meridian (solid arrows in Fig. 5); as α_j is increased, the states S_1 and S_2 approach the "up" and "down" states respectively. At a critical current they merge pairwise and disappear. (2), Increasing magnetic field shifts points $M_{up/down}$ along the meridian towards the field directions and points $S_{1,2}$ away from the field direction (dashed, empty arrows in Fig. 5).

Consider now the situation with a small fixed current and a variable external field. For the discussion we will assume a fixed direction of $\mathbf{h}$ between $+\hat{y}$ and $+\hat{z}$ directions (see Fig. 5). Equations (17) show that as the field magnitude h is increased, the off-meridian states approach the meridian and reach it at a critical field magnitude. Since the two off-meridian states are mirror symmetric with respect to the $y-z$ plane, they reach the meridian simultaneously and merge. Moreover, using Eq. (17) one can show that the merging point also satisfies Eq. (16), so actually a merging of two off-meridian and one on-meridian equilibrium takes place. This tri-equilibrium merging is not accidental. As discussed in Ref. 39, merging of equilibria has to conserve the winding number and it would be impossible for the two off-meridian equilibria with equal winding numbers to merge without the participation of a third equilibrium with the opposite winding number.

As h is increased further, the new equilibrium X, resulting from the merging of S_2, OM_1, and OM_2, remains on-meridian. Analysis in the next section shows that it is an unstable focus, analogous to the maximum energy point equilibrium of a conventional (no spin torque) uniaxial magnet subjected to the external field. In general, above the critical field the evolution of the four on-meridian equilibria M_{up}, M_{down}, S_1, and X is qualitatively similar to that found at $\alpha_j = 0$. We may conclude that our system has two regimes: one at low magnetic field where spin torque dominates, and another one at high field where magnetic torque dominates. The spin torque dominated regime is characterized by the presence of two OM equilibria produced by current. In the

field dominated regime the current-induced equilibria are gone.

These results are quite natural. The SHE system is equivalent to a conventional spin-transfer device with spin polarizer $\mathbf{p}$ directed along $+\hat{x}$.[40] Spin torque attracts the magnetization to $\mathbf{p}$ and repels from $-\mathbf{p}$. At very large currents spin torque dominates all other torques, so, only two equilibrium points — one close $\mathbf{p}$ and another close to $-\mathbf{p}$ should remain. In our system we find that it is enough for the spin torque to dominate the magnetic field torque in order to produce these equilibria. This happens because $\mathbf{p}$ is directed into a point on the equator that is already an equilibrium, albeit unstable, of the the system at zero current.

B. Stability of equilibria analysis and switching phase diagram

In this section we are going to find the critical line $\bar{S}$ of equilibrium destabilization. It will be composed from parts produced by type I and type II solutions.

1. *On-meridian equilibria*

Equations (13) and (14) show that for the on-meridian states λ_{T} is the midpoint of $\lambda_{\pm}$ interval for any current value. Therefore only λ_+ is needed to calculate the critical surface. By substituting $\lambda = \lambda_+(\theta, \phi)$ and $\sin\phi = \pm 1$ into Eqs. (15b) and (15c), we get an exact parametric form of $\bar{S}_M$, the line of on-meridian equilibria destabilization. It turns out to be the same as the one found before[34] using an approximate method.

$$\begin{cases} h_y = \pm \sin^3\theta - \alpha_j \cos\theta \ , \\ h_z = -\cos^3\theta \pm \alpha_j \sin\theta \ . \end{cases} \tag{18}$$

By evaluating $\det A$ and $\mathrm{tr}A$ for each on-meridian equilibrium it is possible to conclude that the "up" and "down" equilibria are stable foci, while the $S_{1,2}$ equilibria are unstable saddle points. The $\bar{S}_M$ curve for various spin torque strengths are shown in Fig. 6.

When magnetic field $\mathbf{h}$ crosses $\bar{S}_M$, one of the stable equilibria $M_{up/down}$ merges with one of the saddles $S_{1,2}$ and disappears. In fact, $\bar{S}_M$ represents the SW astroid boundary modified by the current:[34] The original astroid shape is squeezed along one of the diagonal directions. The segments of $\bar{S}_M$ connecting the corner points of the astroid become unequal: two of them grow with increasing α_j, and the other two shrink. The details of merging depend on whether the long or the short segment is crossed by the field. On the short segment the sign of the m_z component of the disappearing equilibrium is always opposite to the sign of the field component h_z. This property was satisfied everywhere on the conventional SW astroid boundary, and we denote the short segment of $\bar{S}_M$ as $\bar{S}_{Mc}$ with index "c" meaning "conventional". On the long segment the sign of m_z is not determined by the sign of h_z. Indeed, points M_{up} and S_1 merging on this segment have $m_z > 0$, and at the same time it can be crossed by a field with $h_z > 0$, if $\mathbf{h}$ is directed at a small enough angle to the y axis. We denote the long segment as $\bar{S}_{Mu}$ with index "u" meaning "unconventional".

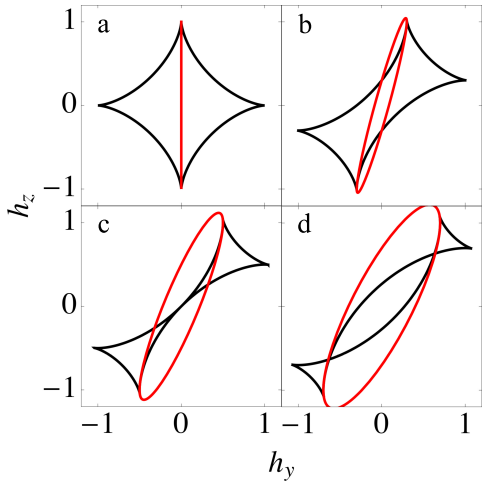

FIG. 6. (color online) Modified astroid composed of $\bar{S}_M$ (black) and $\bar{S}_{OM}$ (red/grey) lines. Spin torque strengths are (a) $\alpha_j = 0$, (b) $\alpha_j = 0.3$, (c) $\alpha_j = 0.5$, (d) $\alpha_j = 0.7$.

2. *Off-meridian equilibria*

Next, we analyze the stability of the off-meridian equilibria. Recall that for them $\lambda = -\cos^2\theta$ and according to Eq. (14) $\lambda \leqslant \lambda_-$ is automatically satisfied when $\lambda_{\pm}$ are real. Thus, according to criteria (12), only the $\bar{S}_T$ critical line is relevant whether $\lambda_{\pm}$ are real or complex, and the stability condition for these states is given by

$$\lambda - \lambda_{\mathrm{T}} = \left(\frac{\alpha_j}{\alpha}\cos\phi - \frac{1}{2}\sin\theta\right)\sin\theta > 0. \tag{19}$$

This inequality can be satisfied only for $\cos\phi > 0$, which means that the OM_2 equilibrium characterized by $\pi/2 \leq \phi \leq 3\pi/2$ is always unstable. The off-meridian equilibrium with $-\pi/2 < \phi < \pi/2$ can be stable. The critical line $\lambda = \lambda_T$ gives a destabilization boundary $\bar{S}_{OM}$ for this equilibrium. Its analytic form is obtained from Eqs. (15b) and (15c) as

$$h_z = \frac{h_y}{\alpha_j} \pm \sqrt{{\alpha_j}^2 - {h_y}^2}\sqrt{1 - \frac{\alpha^2}{4{\alpha_j}^2}\left(1 - \frac{{h_y}^2}{{\alpha_j}^2}\right)} \tag{20}$$

The $\bar{S}_{OM}$ curve for various damping parameters at a fixed spin torque strength is shown in Fig. 7. From $\det A$ and $\mathrm{tr}A$ analysis it is possible to extract more detailed information about the nature of the $OM_{1,2}$ equilibria. We find that inside the domain bounded by the $\bar{S}_{OM}$ line

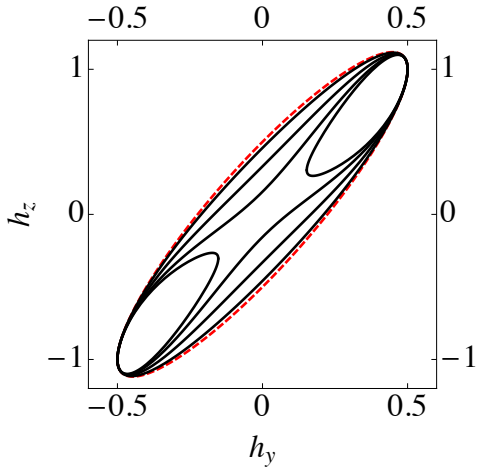

FIG. 7. (color online) $\bar{S}_{OM}$ boundaries for various damping factors with spin torque strength set to $\alpha_j = 0.5$. To make lines distinguishable, we adopt large damping parameters, with α/α_j set to be 0.8, 1.5, 1.9, and 2.1 (going from the outermost to the innermost curves). At low damping regime $\bar{S}_{OM}$ is very close to the boundary of existence of the OM points (red/grey dashed line).

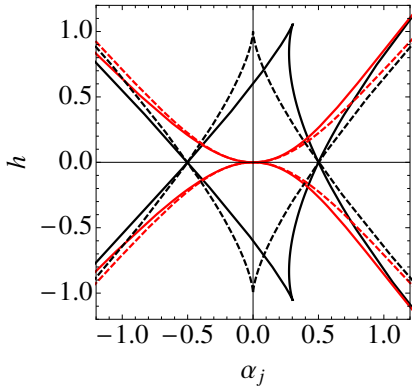

FIG. 8. (color online) Tilted current-field phase diagram at $\alpha = 0$. The black and red(gray) lines correspond to h_{cM} and h_{cOM}, respectively. The solid lines represent the diagrams with a tilting angle of the field set to be 15 degree with respect to $\hat{y}$ direction. The dashed lines represent the diagram with $\mathbf{h}||\hat{y}$. Opposite tilting happens when the angle is negative.

OM_2 is always an unstable node (two real positive eigenvalues), and the OM_1 equilibrium is a stable focus (complex conjugate eigenvalues with negative real parts) — see Appendix C for a complete analysis. As the field increases and moves out of this domain, OM_1 is destabilized but not destroyed. It continues to exist, first as an unstable focus, and then as an unstable node, until it finally merges with the points OM_2 and S_2, as discussed in Sec. IV A. More details of the OM_1 state evolution are provided in Appendix C.

C. Current-field diagrams

Switching phase diagrams Fig. 6 and Fig. 7 describe experiments performed at fixed current with magnetic field of a fixed direction increased until switching happens at a critical value h_c. In a different type of experiment one can measure how the h_c threshold depends on the current magnitude. Such experiments were indeed recently performed by Yu *et al.*[24] (also numerically modelled earlier[35]). The $h_c(\alpha_j)$ dependencies were measured for different field directions and, quite surprisingly, it was found that for fields making a finite angle with the y axis multiple switchings may occur. This fact finds a natural explanation in the framework of our theory. In terms of Fig. 6 the critical fields are determined by the intersections of a straight line representing the field direction with the lines $\bar{S}_M$ and $\bar{S}_{OM}$. If the direction of the field is defined by the angle θ_h with respect to the z-axis, the former intersection point $h_{cM}(\alpha_j)$ can be found by solving Eqs. (18) with $h_y = h_c \sin\theta_h$, $h_z = h_c \cos\theta_h$. For the latter intersection point $h_{cOM}(\alpha_j)$ Eqs. (20) should be used. The results are shown in Fig. 8. One can see that for the field directed along the y-axis ($\theta_h = \pi/2$) the dependence $h_{cM}(\alpha_j)$ exhibits a sharp peak at $\alpha_j = 0$. As the field is tilted away from the y-axis, the position of the peak moves and its initially symmetric shape deforms. Eventually the deformation grows so big that the function $h_{cM}(\alpha_j)$ becomes multi-valued, in accord with experimental findings. Comparing the current-field diagram with the experimental diagram (Fig. 3 of Ref. 24) one can see a good qualitative correspondence.

Here we show how the shape of $h_{cM}(\alpha_j)$ can be understood from the evolution of the modified astroid $\bar{S}_M$. As the current is increased with $\alpha_j > 0$, the astroid is squeezed in the $(1,-1)$ direction and expanded in the $(1,1)$ direction. The $\bar{S}_{Mu}$ lines approach the origin in the h-space and the $\bar{S}_{Mc}$ lines move away from it. When the field is directed along the y axis, its line intersects the $\bar{S}_{Mu}$ boundary. Since this boundary moves towards the origin with increasing α_j, the function $h_{cM}(\alpha_j)$ is decreasing. However, when the field is directed at an angle to the y-axis, its line may initially cross the $\bar{S}_{Mc}$ boundary. Since $\bar{S}_{Mc}$ moves away from the origin, the function $h_{cM}(\alpha_j)$ would increase. At a threshold value of current the field line goes exactly through the corner point between the $\bar{S}_{Mc}$ and $\bar{S}_{Mu}$. At this point $h_{cM}(\alpha_j)$ exhibits a cusp. For currents above the threshold, the field line crosses $\bar{S}_{Mu}$ and, just like in the $\mathbf{h}||\hat{y}$ case, $h_{cM}(\alpha_j)$ becomes a decreasing function. For some angles θ_h there may be situations when the field line crosses both $\bar{S}_{Mc}$ and $\bar{S}_{Mu}$ lines. This is when $h_{cM}(\alpha_j)$ becomes multi-valued and complicated hysteresis patterns are realized.

The form of the other critical field line, $h_{cOM}(\alpha_j)$ (red curves in Fig. 8), is related to the evolution of the $\bar{S}_{OM}$

line. Since this line moves away from the origin in all directions, $h_{cOM}(\alpha_j)$ turns out to be an increasing function.

D. Discussion of the phase diagram

The $\bar{S}_M$ and $\bar{S}_{OM}$ lines together give the complete switching phase diagram in the $y-z$ field plane. For small values of α_j the critical line $\bar{S}_M$ is qualitatively equivalent to the conventional SW astroid, and the equilibrium merging process is similar: There are four on-meridian equilibria for $\mathbf{h}$ inside the astroid, and as the field crosses its boundary two of them merge and disappear. Above the critical current $\alpha_j = 1/2$, the $\bar{S}_M$ critical line becomes self-crossing (Fig. 6). At the critical current the $\bar{S}_{Mu}$ lines touch each other at $\mathbf{h} = 0$, so, the threshold can be found from Eq. (18) with $h_y = h_z = 0$. Inside the region of self-crossing there are no on-meridian equilibria, as already observed in Ref. 34 and the supplemental material of Ref. 7. However, the Poincaré-Hopf theorem is not violated due to the presence of the off-meridian equilibria.

In the absence of current the system in constant external field $\mathbf{h}$ resides in one of the two stable M equilibria. As α_j is increased, the oval-shaped region of stability of the OM_1 state grows, and the area inside the modified astroid $\bar{S}_M$ shrinks. Moreover, the self-crossing region of $\bar{S}_M$, where no on-meridian equilibria exist, also grows. Thus both M_{up} and M_{down} states eventually become unstable at some critical currents α_j^{Mup} (α_j^{Mdown}) and $\mathbf{m}$ switches to the OM_1 state. What happens if the current is subsequently decreased? The answer to this question can be read from the $h_c(\alpha_j)$ dependence shown in Fig. 8. At a given h the off-meridian state remains stable down to the current α_j^{OM} obtained from the equation $h = h_{cOM}(\alpha_j)$. If $\alpha_j^{OM} < \alpha_j^M$, one would observe hysteretic behavior of the system in the current interval between α_j^{OM} and α_j^M. At the higher end of this interval the system switches from an M state to the OM_1 state. At the lower end it switches back to an M state. As seen from Fig. 8, the length of the bistable interval becomes larger for smaller h. At $\mathbf{h} = 0$ using Eq. (20) one finds $\alpha_j^{OM}|_{h=0} = \alpha/2$. The value of α_j^M at $\mathbf{h} = 0$ was already discussed — it corresponds to the first self-crossing of $\bar{S}_M$, thus $\alpha_j^M|_{h=0} = 1/2$. For typical values of Gilbert damping $\alpha \sim 0.01$ the hysteresis range is very large. It requires an initial pulse of current of the order $\alpha_j \sim 1$ to get to the OM state, but after that the current can be reduced to $\alpha_j \sim \alpha$, and the OM state can be comfortably studied at low currents. Experiments with SHE devices[5,7] are already performed in the regime $\alpha_j \sim 1$ so the discussed hysteresis should be observable.

When magnetic field is set inside the domain of existence of OM states but outside of their domain of stability, the system has two unstable OM equilibria. It is possible to arrange parameters so that there no M equilibria either (this happens in the high damping, high current regime). In this case the system has no choice but to follow some precession cycle, the analysis of which is beyond the scope of the present paper.

V. DYNAMIC PROPERTIES

In this section we discuss what happens after the stability boundaries are crossed and equilibria are destabilized.

A. Switching to the off-meridian state

Existence of a stable OM state within the area given by Eqs. (20) raises a question: When an M state is destabilized at the $\bar{S}_M$ boundary, will the system switch to the other M state, or to a stable OM state? To answer this question we plot the flow diagrams (phase portraits) of the system. The results of simulations are presented in the form of qualitative sketches that emphasize the structure of the flow (Fig. 9).

In the field-dominated regime the flow is qualitatively similar to that in the absence of the current. There are two basins of attraction of stable points M_{up} and M_{down} (white and grey areas in Fig. 9(a)). The separatrix between the two basins winds around the unstable focus X making an infinite number of turns. As a result, near X the basins are finely intermixed and a small change in initial conditions may change the equilibrium where the system ends up. When the modified astroid boundary is crossed, one of M points is destroyed. A system initially residing in this point will switch to the other M point.

Simulations in the current-dominated regime show three basins of attraction. The one of the OM_1 point (darkest area in Fig. 9(b)) separates those of M_{up} (white area) and M_{down} (grey area). The white and grey areas touch at the point of unstable equilibrium OM_2. The important difference from the field-dominated regime is that OM_2 is an unstable node, and not a focus. Thus, there is no winding of the separating line around it and, consequently, no area of fine intermixing. Fig. 9(c) shows what happens when the current is increased further so that M_{up} and S_1 merge at the modified astroid boundary. The phase portrait in the upper part of the unit sphere qualitatively changes: The basins of attraction of M_{up} and OM_1 merge, forming a larger basin of attraction of OM_1. This transformation of the phase portrait does not affect the qualitative picture in the lower part of the unit sphere and the boundary between the basin of OM_1 and M_{down}. The end result is that a system initially residing in M_{up} will switch to the OM_1 state with certainty. The latter statement, of course, only applies to the case of slow, quasi-static change of parameters, in which case one can be sure that $\mathbf{m}$ follows the stable point with great accuracy. If parameters are changed at a finite speed, there will be a lag between $\mathbf{m}$ and the equilibrium point, and a more careful investigation is necessary.

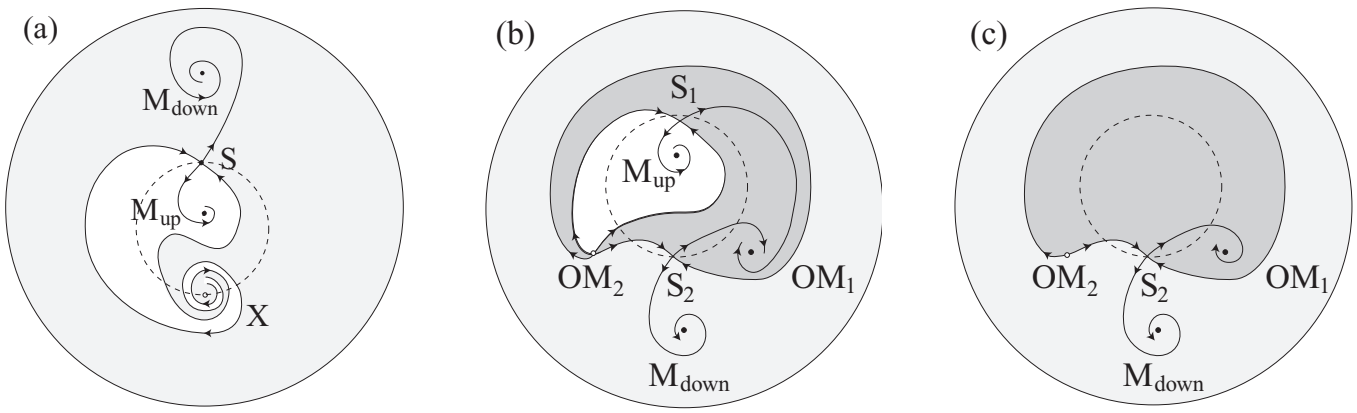

FIG. 9. Sketches of the phase portraits on the stereographic plane describing the evolution of the system in a constant field $\mathbf{h} = +h\hat{y}$ with increasing current. The north and south poles are projected to the circle center and to infinity, respectively; the dashed circle is the projection of the equator. (a) Field-dominated regime. Two basins of attraction exist for the M_{up} and M_{down} equilibria. (b) Current-dominated regime with the additional $OM_{1,2}$ equilibria. The basins of attraction of M_{up} and M_{down} are separated by the basin of attraction of OM_1. Spin torques had shifted M_{down} trough the South pole and it shows up in a different place on the stereographic plane. (c) Further increase of current results in the merging of M_{up} and S_1. The magnetization finds itself in the basin of attraction of OM_1 and switches to the off-meridian state. A set of phase portraits that represents the three cases above can be obtained with parameters: (a)$h_y < 1$, $\alpha_j = 0$; (b)$h_y = 0.05$, $\alpha_j = 0.3$; and (c) $h_y = 0.15$, $\alpha_j = 0.45$.

B. Two-stage switching through the off-meridian equilibrium

Magnetization reversal is one of the most important processes in magnetism that is linked to the magnetic data storage process, such as in hard disk drives. Switching speed and reliability are two crucial factors to the design of such systems. In conventional spin-transfer torque switching spin polarizer is directed along the easy axis of the free layer. Then the magnetization moves towards the new equilibrium along a spiral trajectory in a reliable but fairly slow manner.[22,41–45] Much faster reversals, which are often called precessional switchings, have been designed. Some have magnetic field applied orthogonally to the easy axis. Others use spin polarizer perpendicular to the easy plane of the free layer ("magnetic fan" geometry).[46–48] In both cases the reversal processes is fast but requires current or field pulse length to be carefully adjusted. This is experimentally hard to achieve, consequently such methods may lead to greater error rates.

It was numerically found[35,37] that switching from an M state to the OM_1 state happens fast, without precession or "ringing". A recent micromagnetic simulation[49] confirmed that this result is not an artefact of the macrospin approximation. Figure 10 shows the process of switching from M_{up} to OM_1 state. It is seen that the switching time is of the order of ferromagnetic resonance period T ($T = 2\pi$ in dimensionless unit used in Fig. 10). In the framework of our theory the absence of precession is explained as follows. Switching is initiated by the destruction of an M equilibrium due to its merging with an S point. Since in the current-dominated regime there is no fine intermixing of the basins of attractions, the flow lines originating from the merging point do not exhibit a winding pattern, and consequently there are no oscillations in the beginning of the switching process. Oscillations at the end of switching process, when $\mathbf{m}$ approaches the focus OM_1, are suppressed for another reason. In order to cause a merging of M and S spin torque has to be large with $\alpha_j \sim 1$. But a large spin torque strongly increases the effective damping, especially since the damping action achieves its maximum at the position of OM_1.[39] This is why, while strictly speaking OM_1 is a focus, oscillations are almost absent in practice.

Is it possible to utilize the fast nature of the $M_{up} \to OM_1$ switching to achieve a useful and fast procedure for transitions between the zero-current states M_{up} and M_{down}? We will consider one possible $M_{up} \to M_{down}$ switching scenario with an intermediate stop in the OM_1 state. Consider a system that is initially in the M_{up} state. Magnetic field $\mathbf{h}$ is set in the negative z direction during the whole switching procedure with its magnitude satisfying $h < 1$, so that $M_{up} = +\hat{z}$ state remains stable. First, we apply a short pulse of strong current $\alpha_j \sim 1$. The rise and fall times of the pulse are assumed to be negligible. During the pulse time M_{up} does not exist and $\mathbf{m}$ switches to OM_1. The pulse length t_p is selected to be large enough for the switching process bo be accomplished. Importantly, this requirement sets only a low bound for t_p — there will be no harm in keeping the current switched on for a longer time. According to Eqs. (20) for $h_y = 0$ the state OM_1 has $\theta = \pi/2$ and sits on the equator of the unit sphere. After the end of the pulse the current is switched off and the second stage of switching begins. Now the states M_{up} to M_{down} are

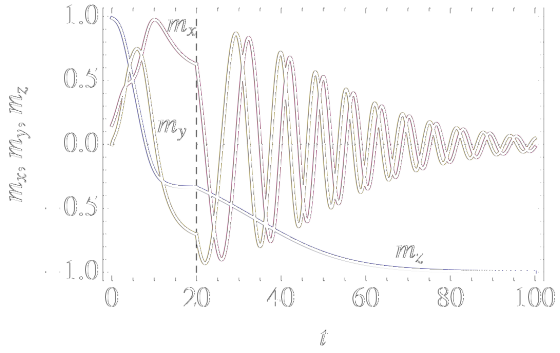

FIG. 10. (color online) Evolution of the three components of the magnetization in a two stage switching process by direct numerical integration of LLG equation. The parameters are: $h_y = 0.15$, $\alpha_j = 0.45$, and $\alpha = 0.05$. The field-current pulse is turned on at $t = 0$ and off at $t = 20$.

stable again and **m** should go to one of them. With field pointing down and $\alpha_j = 0$, the boundary between the basins of attraction of M_{up} and M_{down} is a parallel circle, located above the equator of the unit sphere. Thus the second stage starts with **m** residing in the basin of attraction of M_{down}, to which **m** eventually relaxes in a precessional manner. The whole process is characterized by a fast first stage with strong current and a slow second stage, during which the systems is not driven externally. While the total switching time is of the same order of magnitude as in the conventional switching, the "active" stage requires much shorter time, comparable to that of precessional switching, making the procedure potentially useful for special applications. An important drawback of this switching scenario is that for a given direction of **h** it can be performed only in one direction, e.g., in the discussion above from M_{up} to M_{down}. To switch back one would have to reverse the direction of **h**.

It is interesting to to note that the SHE device switching between M_{up} and M_{down} in a two-stage manner described above can be alternatively viewed as a realization of a controlled-NOT gate with h_z being the control parameter.

Finally, we want to compare the duration of the fast stage of SHE switching with the switching time of a conventional spin-torque device, where the magnetic polarizer and the external field are both pointing along the easy axis of the free layer. Assuming the conventional spin torque to be described by a constant spin-transfer efficiency factor $g(\theta) = \bar{g}$, we get $\mathbf{h}_{sp} = \alpha_j[\mathbf{m} \times \hat{z}]$ with $\alpha_j = \bar{g}j/j_0$ for its effective field. In this fully axially-symmetric case the switching time can be computed analytically[50] as

$$t_s = \frac{1}{2\alpha(1-h')} \ln\left(\frac{1-m_{z0}}{1-m_{z0}/h'}\right), \qquad (21)$$

with $h' = h + \alpha_j/\alpha$ and m_{z0} being the initial value of the magnetization component along the easy axis. In the small-damping ($\alpha \ll 1$), large-current ($\alpha_j/\alpha \gg h \sim 1$), regime this simplifies to $t_s \approx -\ln(1-m_{z0})/(2\alpha_j)$. Spin torque switching in collinear geometry requires some initial deviation of **m** from equilibrium. This deviation is usually thought to come from thermal fluctuations and can be evaluated by using Maxwell equilibrium distribution for m_{z0}

$$\rho(m_{z0}) = \kappa\sqrt{1-m_{z0}^2}\, e^{-E(m)/k_bT}. \qquad (22)$$

where κ is the normalizing constant. To compare the switching times we adopt a typical expected value at room temperature of $m_{z0} \approx 0.99$ ($\theta_0 \approx 0.5^\circ$).[51] For the purpose of switching time comparison it is important to remember that conventional and SHE devices differ in two aspects. On the theoretical level, in conventional devices switching occurs at $\alpha_j \sim \alpha$, while $\alpha_j \sim 1$ is required for SHE switching. On a practical level conventional devices can bear smaller currents due to heating problems. Thus achieving $\alpha_j \sim 1$ in them is problematic. In view of that, we perform two comparisons. First, we compare the SHE and conventional switching times for $\alpha_j = 0.5$ and $h = 0$. Here we get $t_p \approx 14$ and $t_s \approx 5$. Given the same normalized spin torque strength, conventional device is faster than the SHE one. Second, we compare the two devices operating at their critical switching current with a small field, say $h = 0.02$, pointing toward the $-z$ direction. For the SHE device we again use $\alpha_j = 0.5$ and the resulting switching time does not change much, $t_p \approx 13.5$. For a conventional devices we use $\alpha_j = \alpha$, then $t_s \approx 29/\alpha$. In this sense the SHE switching turns out to be much faster. In addition, since the initial condition is a statistical average, the switching time estimated in this fashion may cause a non-negligible error in experiments.

VI. SUMMARY

We considered magnetic switching in a bilayer F/N structure with strong spin-orbit interaction using a macrospin approximation that is applicable to sufficiently small, single domain devices. The method of Refs. 32 and 33 provides a framework that can be applied to find the critical switching surfaces for any magnetic single domain system with arbitrary anisotropy and spin torque in an exact fashion. In this article we calculated the three-dimensional critical surface for a SHE bilayer system with perpendicular anisotropy and in-plane current using single domain approximation. For external fields in the $y-z$ plane, the SHE induced spin torque not only shifts the existing equilibria, but also generates two new, current-induced equilibria.

First, we derive an analytic formula for the stability boundary for the current-induced equilibria — in previous numeric research this boundary was not distinguished from the boundary of its existence. *Second*, in contrast to the other authors we discuss the switching phase diagrams in the field space at a constant current, and plot the modified astroid and the oval-shaped stability region of the off-meridian state. We then show how our

qualitative description of the evolution of the constant current switching boundaries can explain the results of the other authors obtained for variable currents. *Third*, we discuss in detail the evolution of equilibrium points and the character of their destabilization on the switching boundaries. This allows us to put forward a qualitative understanding of the complicated hysteresis processes that are found in SHE devices. *Fourth*, we point out that while a large current is required to set magnetization into the current-induced state, it remains in this state when current is decreased to values that are α times smaller. Thus spin-torque induced state can be studied at low currents. *Fifth*, we show that in the current-dominated regime switching between "up" and "down" equilibria can deterministically proceed through the current-induced state. The first stage of this switching is very fast, without ringing effects in the beginning or at the end, and an explanation to this fact is provided. An example of two-stage switching is considered and the switching time is compared to that of a conventional collinear spin-torque device with magnetic polarizer. Here it is found that, depending on the limitations on current magnitude imposed by the factors not related to spin torque physics, either of the two devices can operate faster.

ACKNOWLEDGMENTS

This research was supported by National Science Foundation Grant No. DMR-0847159.

Appendix A

The explicit expression of each component in Eq. (9) can be derived as

$$\partial_\theta f^\theta = -\partial_{\theta\theta}\varepsilon + \partial_\theta {h_{\rm sp}}^\theta, \tag{A1a}$$

$$\partial_\theta f^\phi = -\partial_\theta\left(\frac{1}{\sin\theta}\partial_\phi\varepsilon\right) + \partial_\theta {h_{\rm sp}}^\phi, \tag{A1b}$$

$$\partial_\phi f^\theta = \frac{\cos\theta}{\sin\theta}\left(\frac{1}{\sin\theta}\partial_\phi\varepsilon - {h_{\rm sp}}^\phi\right) - \frac{1}{\sin\theta}\left(\partial^2_{\theta\phi}\varepsilon - \partial_\phi {h_{\rm sp}}^\theta\right), \tag{A1c}$$

$$\partial_\phi f^\phi = -\frac{\cos\theta}{\sin\theta}\left(\partial_\theta\varepsilon - {h_{\rm sp}}^\theta\right) - \frac{1}{\sin^2\theta}\partial^2_{\phi\phi}\varepsilon + \frac{1}{\sin\theta}\partial_\phi {h_{\rm sp}}^\phi. \tag{A1d}$$

Appendix B

For a planar linear system of the form $\dot{\mathbf{X}} = A\mathbf{X}$, the eigenvalues of the 2×2 coefficient matrix A can be calculated in terms of its trace and determinant as[38]

$$\mu_\pm = \frac{1}{2}\left(\mathrm{tr}A \pm \sqrt{(\mathrm{tr}A)^2 - 4\mathrm{det}A}\right). \tag{B1}$$

Therefore knowing $\mathrm{tr}A$ and $\mathrm{det}A$ tells us virtually everything about the geometry of its solutions.

Besides stability, the types of an equilibrium is also of importance in understanding the switching process. An equilibrium of the same stability (except saddle point) can be a node or a focus, depending on whether the eigenvalues (B1) are real or complex. Therefore the differentiation of the focus set and the node set requires another pair of critical values $\lambda_{c\pm}$ which satisfies

$$(\mathrm{tr}A)^2 - 4\mathrm{det}A = 0. \tag{B2}$$

It can be demonstrated that the relationships $\lambda_{c+} \geqslant \lambda_+$ and $\lambda_{c-} \leqslant \lambda_-$ are always satisfied.

The classification of stability and equilibrium type in terms of the eigenvalues and λ are summarized in TABLE I and in TABLE II, respectively. The complete dynamic analysis of an equilibrium needs to take into account the two factors together.

Appendix C

We mentioned the equilibrium types of the two off-meridian equilibrium states and their evolution in Sec. IV A and in Sec. IV B 2. To quantitatively understand the evolution of these two states, we also need to find the critical λ which separates nodes and foci, i.e., to solve Eq. (B2). It's solution in the off-meridian case is given by

$$\lambda_{\rm c\pm} = \frac{\sin^2\theta}{2} - \cos^2\theta \pm \frac{1}{2}\sin^2\theta\sqrt{1+\alpha^2} + \alpha_j\alpha\sin\theta\cos\phi. \tag{C1}$$

The two critical values $\lambda_{\rm c\pm}$ give another two surfaces in the parameter space, one above λ_+ and the other below λ_-. Since both the two off-meridian equilibria have $\lambda \equiv -\cos^2\theta < \lambda_-$, we only need $\lambda_{\rm c-}$ to determine the equilibrium type.

The two off-meridian equilibrium have different equilibrium types. For the one with $\pi/2 < \phi < 3\pi/2$, we have $\lambda_- \geqslant \lambda \geqslant \lambda_{\rm c-}$, therefore it is always an unstable node. The other one which satisfies $-\pi/2 < \phi < \pi/2$ may change the equilibrium type as field changes. we can find two critical curves by equating λ to λ_- and to $\lambda_{\rm c-}$, respectively. The former gives the destabilization boundary $\bar{S}_{OM}$, the latter corresponds to the type transition boundary $\bar{S}_c$ of the analytic form

$$h_z = \frac{h_y}{\alpha_j} \pm \sqrt{\alpha_j^2 - h_y^2}\sqrt{1 - \frac{\left(\sqrt{\alpha^2+1}-1\right)^2}{4\alpha^2\alpha_j^2}\left(1 - \frac{h_y^2}{\alpha_j^2}\right)}. \tag{C2}$$

TABLE I. Classification of stability

Stability Type	Equilibrium Type	Eigenvalue Equivalent	tr$A$-det$A$ Equivalent	λ Equivalent
Sink	Stable focus Stable node	Complex Re$[\mu_\pm] < 0$ Real $\mu_- < \mu_+ < 0$	tr$A < 0$, det$A > 0$	$\begin{cases} \lambda > \mathrm{Max}(\lambda_\mathrm{T}, \lambda_+) & \text{if } \lambda_\mathrm{T} \geqslant \lambda_- \\ \lambda_\mathrm{T} < \lambda < \lambda_- & \text{if } \lambda_\mathrm{T} < \lambda_- \end{cases}$
Source	Unstable focus Unstable node	Complex Re$[\mu_\pm] > 0$ Real $0 < \mu_- < \mu_+$	tr$A > 0$, det$A > 0$	$\begin{cases} \lambda < \mathrm{Min}(\lambda_\mathrm{T}, \lambda_-) & \text{if } \lambda_\mathrm{T} \leqslant \lambda_+ \\ \lambda_+ < \lambda < \lambda_T & \text{if } \lambda_\mathrm{T} > \lambda_+ \end{cases}$
Saddle	Saddle point	Real $\mu_- < 0 < \mu_+$	det$A < 0$	$\lambda_- < \lambda < \lambda_+$

TABLE II. Classification of focus and node

Equilibrium Type	Eigenvalues	tr$A$-det$A$ Equivalent	λ Equivalent
Node	Real	$(\mathrm{tr}A)^2 - 4\mathrm{det}A > 0$, det$A > 0$	$\lambda_{c-} < \lambda < \lambda_-$ or $\lambda_+ < \lambda < \lambda_{c+}$
Focus	Complex	$(\mathrm{tr}A)^2 - 4\mathrm{det}A < 0$ [a]	$\lambda < \lambda_{c-}$ or $\lambda > \lambda_{c+}$

[a] Note that $(\mathrm{tr}A)^2 - 4\mathrm{det}A < 0$ guarantees det$A > 0$.

The transition boundary $\bar{S}_c$ touches $\bar{S}_{OM}$ but never crosses it. It separates the unstable region of the off-meridian equilibrium into node and focus regions, as shown in Fig. 11.

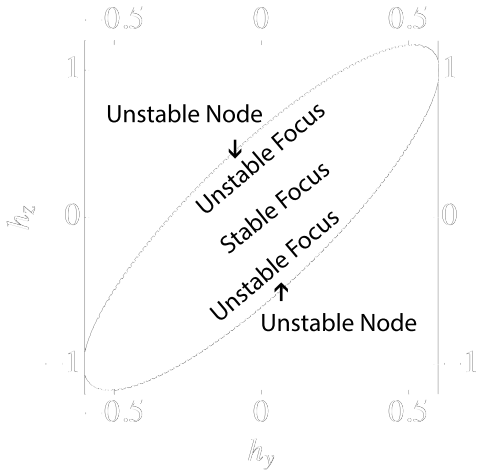

FIG. 11. The $\bar{S}_{OM}$, $\bar{S}_c$, and the equilibrium merging boundary are plotted with solid, dashed, and dotted lines, respectively. The unstable node, unstable focus, and stable focus regions are marked in different grayscales. For illustrative purposes, we adopt $\alpha_j = 0.6$ and $\alpha = 1$ to make the unstable regions large enough to be seen.

* syan@physics.sc.edu
† yar@physics.sc.edu

[1] K. Ando, S. Takahashi, K. Harii, K. Sasage, J. Ieda, S. Maekawa, and E. Saitoh, Phys. Rev. Lett. **101**, 036601 (2008).
[2] I. M. Miron, G. Gaudin, S. Auffret, B. Rodmacq, A. Schuhl, S. Pizzini, J. Vogel, and P. Gambardella, Nat. Mater. **9**, 230 (2010).
[3] U. H. Pi, K. Won Kim, J. Y. Bae, S. C. Lee, Y. J. Cho, K. S. Kim, and S. Seo, Appl. Phys. Lett. **97**, 162507 (2010).
[4] L. Liu, T. Moriyama, D. C. Ralph, and R. A. Buhrman, Phys. Rev. Lett. **106**, 036601 (2011).
[5] I. M. Miron, K. Garello, G. Gaudin, P.-J. Zermatten, M. V. Costache, S. Auffret, S. Bandiera, B. Rodmacq, A. Schuhl, and P. Gambardella, Nature **476**, 189 (2011).
[6] Z. Wang, Y. Sun, M. Wu, V. Tiberkevich, and A. Slavin, Phys. Rev. Lett. **107**, 146602 (2011).
[7] L. Liu, O. J. Lee, T. J. Gudmundsen, D. C. Ralph, and R. A. Buhrman, Phys. Rev. Lett. **109**, 096602 (2012).
[8] L. Liu, C.-F. Pai, Y. Li, H. Tseng, D. Ralph, and R. Buhrman, Science **336**, 555 (2012).
[9] C.-F. Pai, L. Liu, Y. Li, H. Tseng, D. Ralph, and R. Buhrman, Appl. Phys. Lett. **101**, 122404 (2012).
[10] J. Kim, J. Sinha, M. Hayashi, M. Yamanouchi, S. Fukami, T. Suzuki, S. Mitani, and H. Ohno, Nat. Mater. (2012).
[11] Y. A. Bychkov and E. I. Rashba, Journal of physics C: Solid state physics **17**, 6039 (1984).
[12] A. Manchon and S. Zhang, Phys. Rev. B **78**, 212405 (2008).
[13] A. Manchon and S. Zhang, Phys. Rev. B **79**, 094422 (2009).
[14] A. Matos-Abiague and R. Rodriguez-Suarez, Phys. Rev. B **80**, 094424 (2009).
[15] P. Gambardella and I. M. Miron, Philosophical Transactions of the Royal Society A: Mathematical, Physical and Engineering Sciences **369**, 3175 (2011).
[16] P. M. Haney, H.-W. Lee, K.-J. Lee, A. Manchon, and M. D. Stiles, Phys. Rev. B **88**, 214417 (2013).
[17] J. E. Hirsch, Phys. Rev. Lett. **83**, 1834 (1999).
[18] S. Zhang, Phys. Rev. Lett. **85**, 393 (2000).
[19] J. Sinova, D. Culcer, Q. Niu, N. A. Sinitsyn, T. Jungwirth, and A. H. MacDonald, Phys. Rev. Lett. **92**, 126603 (2004).
[20] T. Jungwirth, J. Wunderlich, and K. Olejník, Nat. Mater. **11**, 382 (2012).
[21] J. C. Slonczewski, J. Magn. Magn. Mater. **159**, L1 (1996).
[22] D. Ralph and M. D. Stiles, J. Magn. Magn. Mater. **320**, 1190 (2008).
[23] P. M. Haney, H.-W. Lee, K.-J. Lee, A. Manchon, and M. D. Stiles, Phys. Rev. B **87**, 174411 (2013).
[24] G. Yu, P. Upadhyaya, K. L. Wong, W. Jiang, J. G. Alzate, J. Tang, P. K. Amiri, and K. L. Wang, Phys. Rev. B **89**, 104421 (2014).
[25] K.-W. Kim, S.-M. Seo, J. Ryu, K.-J. Lee, and H.-W. Lee, Phys. Rev. B **85**, 180404 (2012).
[26] D. A. Pesin and A. H. MacDonald, Phys. Rev. B **86**, 014416 (2012).
[27] X. Wang and A. Manchon, Phys. Rev. Lett. **108**, 117201 (2012).
[28] O. Lee, L. Liu, C. Pai, Y. Li, H. Tseng, P. Gowtham, J. Park, D. Ralph, and R. Buhrman, Phys. Rev. B **89**, 024418 (2014).
[29] S. Emori, U. Bauer, S.-M. Ahn, E. Martinez, and G. S. Beach, Nat. Mater. **12**, 611 (2013).
[30] K.-S. Ryu, L. Thomas, S.-H. Yang, and S. Parkin, Nature nanotechnology **8**, 527 (2013).
[31] E. C. Stoner and E. Wohlfarth, Philosophical Transactions of the Royal Society of London. Series A. Mathematical and Physical Sciences , 599 (1948).
[32] A. Thiaville, Phys. Rev. B **61**, 12221 (2000).
[33] S. Yan, Z. Sun, and Y. B. Bazaliy, Phys. Rev. B **88**, 054408 (2013).
[34] J. H. Chang, H. H. Chen, and C. R. Chang, Phys. Rev. B **83**, 054425 (2011).
[35] J.-H. Chang, H.-H. Chen, and C.-R. Chang, Magnetics, IEEE Transactions on **47**, 3876 (2011).
[36] J.-H. Chang, H.-H. Chen, and C.-R. Chang, Journal of Physics D: Applied Physics **46**, 035002 (2013).
[37] K.-S. Lee, S.-W. Lee, B.-C. Min, and K.-J. Lee, Appl. Phys. Lett. **102**, 112410 (2013).
[38] M. W. Hirsch, S. Smale, and R. L. Devaney, *Differential equations, dynamical systems, and an introduction to chaos*, Vol. 60 (Academic press, 2004).
[39] I. Sodemann and Y. B. Bazaliy, Phys. Rev. B **84**, 064422 (2011).
[40] W. H. Rippard, A. M. Deac, M. R. Pufall, J. M. Shaw, M. W. Keller, S. E. Russek, G. E. W. Bauer, and C. Serpico, Phys. Rev. B **81**, 014426 (2010).
[41] G. Bertotti, I. Mayergoyz, C. Serpico, and M. Dimian, J. Appl. Phys. **93**, 6811 (2003).
[42] Y. B. Bazaliy and A. Stankiewicz, Appl. Phys. Lett. **98**, 142501 (2011).
[43] Y. B. Bazaliy, J. Appl. Phys. **110**, 063920 (2011).
[44] R. Koch, J. Katine, and J. Sun, Phys. Rev. Lett. **92**, 088302 (2004).
[45] J. Sun, Phys. Rev. B **62**, 570 (2000).
[46] M. Bauer, J. Fassbender, B. Hillebrands, and R. Stamps, Phys. Rev. B **61**, 3410 (2000).
[47] A. Kent, B. Ozyilmaz, and E. Del Barco, Appl. Phys. Lett. **84**, 3897 (2004).
[48] H. Liu, D. Bedau, D. Backes, J. Katine, J. Langer, and A. Kent, Appl. Phys. Lett. **97**, 242510 (2010).
[49] G. Finocchio, M. Carpentieri, E. Martinez, and B. Azzerboni, Appl. Phys. Lett. **102**, 212410 (2013).
[50] S. Yan, *Nonlinear Magnetic Dynamics and The Switching Phase Diagrams in Spintronic Devices*, Ph.D. thesis, University of South Carolina (2014).
[51] M. d'Aquino, *Nonlinear magnetization dynamics in thin-films and nanoparticles*, Ph.D. thesis, PhD thesis, Universita degli studi di Napoli "Federico II", Facolta di Ingegneria, 2004. URL http://www. fedoa. unina. it/148 (2004).